On the behavior of two C1 finite elements versus anisotropic diffusion

Blaise Faugeras, Hervé Guillard, Boniface Nkonga, Francesca Rapetti

Received: Added at production | Revised: Added at production | Accepted: Added at production

DOI: xxx/xxxx

ARTICLE TYPE

On the behavior of two C1 finite elements versus anisotropic diffusion

Blaise Faugeras[1,2] | Hervé Guillard[1,2] | Boniface Nkonga[1,2] | Francesca Rapetti[1,2]

[1]Département de Mathématiques, Université Côte d'Azur, Parc Valrose, 06108 Nice, France
[2]CASTOR Project Team, Centre Inria Université Côte Azur, Rte des Luciolles, BP 93 06092 Sophia-Antipolis, France

Correspondence
*F. Rapetti Email: francesca.rapetti@univ-cotedazur.fr

Summary

Heat transfer in magnetically confined plasmas is characterized by extremely high anisotropic diffusion phenomena. At the core of a magnetized plasma, the heat conductivity coefficients in the parallel and perpendicular directions of the induction field can be very different. Their ratio can exceed 10^8 and the pollution by purely numerical errors can make very difficult the simulation of the heat transport in the perpendicular direction. Standard numerical methods, generally used in the discretization of classical diffusion problems, are rather inefficient.

The present paper analyses a finite element approach for the solution of a highly anisotropic diffusion equation. Two families of finite elements of class $\mathcal{C}^1$, namely bi-cubic Hemite-Bézier and reduced cubic Hsieh-Clough-Tocher finite elements, are compared. Their performances are tested numerically, for various ratios of the diffusion coefficients, on different mesh configurations, even aligned with the induction field. The time stepping is realised by an implicit high-order Gear finite difference scheme. An example of reduced model is also provided in order to comment on some obtained results.

MSC: 65N30

KEYWORDS:
Anisotropic diffusion, reduced model, isoparametric finite elements, reduced Hsieh-Clough-Tocher finite elements, Hermite-Bézier finite elements, Gear schemes.

1 | INTRODUCTION

Numerical diffusion occurs when the computational method cannot handle high differences in the problem coefficients (as in presence of flow anisotropy), or when it is not able to describe shocks or even when the computational mesh for the simulated domain is not adapted to underline the main features of the considered phenomena. In the framework of magneto-hydro-dynamic (MHD) applications, for example, the length and time scales in a nuclear fusion plasma are interested by extreme variations (see, e.g., [1,2,3,4]), hence numerical methods have not only to be accurate but also robust throughout the different parameter ranges. An example of this heterogeneity, that we consider in these pages, is the anisotropy of the heat conductivity in diffusive processes. In presence of a strong magnetic induction

$\mathbf{B}$, in the core of a fusion plasma, the temperature gradient occurs mainly along the transversal direction (perpendicular to $\mathbf{B}$). In the direction parallel to $\mathbf{B}$, the temperature does not change significantly. Indeed, as explained in [5,6], in the case of a strong confining magnetic induction $\mathbf{B}$, as in tokamak plasmas, the motion of charged particles yields a slow transport perpendicular to the field while particles can travel comparatively long distances parallel to the field before undergoing a collision. In other words, particles are relatively free to move in the direction parallel to the field, but exhibit gyro-orbits in the directions perpendicular to the field.

From the mathematical point of view, this anisotropy puts strong constraints on numerical methods to be used. There is a considerable simplification and accuracy to be gained in either adopting an asymptotic approach (see, e.g., [7,8,9] and the therein references) or numerical high-order methods which uses a coordinate system aligned with the magnetic field (see, e.g., [10]). In [8], an asymptotic preserving method is designed to give a precise solution in the various regimes with no restrictions on the computational meshes. The main point with this technique is to identify the limit model, either by singular perturbation [7] or solution decomposition [8]. Meshes aligned on the equilibrium magnetic flux lines, associated with an isoparametric finite element formulation, offer decisive advantages. The bi-cubic Hermite-Bézier elements [10] allow for an accurate description of the magnetic topology using flux-aligned grids. In addition, the use of this kind of grid is particularly important to control artificial diffusion perpendicular to the flux surfaces that we discuss in these pages, which may spoil the computation of the physical one. At the equilibrium, plasma moves very little. Even if the mesh goes out from alignment, it still remains a good mesh to compute neighbouring equilibria if we adopt numerical approaches (as those considered here) that maintain sufficient accuracy in case of anisotropy. If the plasma moves out abruptly from the equilibrium, it means that we are facing plasma disruption and everything stops (the computation and the plasma). Non aligned meshes allow for an unequalled flexibility in discretizing geometries of any shape and an analysis of numerical diffusion for this type of meshes is presented in [11]. Composite meshes come into play if the alignment to flux surface is desired in the whole plasma domain since the chamber wall is not a magnetic flux surface. We can adopt the mortar method for composite meshes described in [12,13] with rHCT and HB FEs. The goal of the present paper is not to perform an asymptotic analysis of the model problem for a suitable parameter $\epsilon \to 0$ but to analyse the accuracy, of two $\mathcal{C}^1$ high order methods, the reduced Hsieh-Clough-Tocher (rHCT) and the cubic Hermite-Bézier (HB) finite element (FE) approaches, when applied to discretize anisotropic linear operators on different meshes. Note that cubic-Hermite finite element interpolation schemes have been popular also in other research areas, such as in cardiac modeling [14], porous media [15,16], because of their convergence properties in finite element simulations and their ability to capture smooth geometries compactly. However, construction of cubic-Hermite geometric meshes has been often limited to plane geometries due to difficulties in handling complex topologies.

The rest of the paper is organized as follows[1]. We start by stating in Section 2 the problem and its formulation in the continuous setting. We also present an example of model reduction which is useful to comment on some of the numerical results contained in Section 5. In Section 3, we briefly recall the reduced Hsieh-Clough-Tocher element [17] on triangles and the isoparametric bi-cubic Hermite-Bézier

[1] Abbreviations: Degrees of freedom (dofs), Hermite-Bézier (HB), reduced Hsieh-Clough-Tocher (rHCT), Finite elements (FEs).

one on quadrangles. We are then able to state the discrete problem in Section 4 together with its possible variants. We conclude in Section 5 with some numerical results.

2 | SETTING UP THE MODEL PROBLEM.

In a bounded domain $\Omega \subset \mathbb{R}^2$ with smooth boundary $\partial\Omega$ and outward normal $\mathbf{n}$, we consider the anisotropic linear diffusion problem

$$\partial_t u + \nabla \cdot \mathbf{q} = f, \qquad \mathbf{q} = -\mathbb{D}\nabla u, \qquad \forall\, (\mathbf{x}, t) \in \Omega \times [0, T], \qquad T > 0, \tag{1}$$

where u represents the (unknown) temperature, $\mathbf{q}$ the heat flux, f a source term and $\mathbb{D}$ the diffusion 2-tensor. Let $\partial\Omega = \Gamma_D \cup \Gamma_N$ with $\text{mes}(\Gamma_D) > 0$ and $\Gamma_N = \partial\Omega \setminus \Gamma_D$. Problem (1) is here completed by boundary conditions of Dirichlet or Neumann type such as

$$u = u_D \quad \text{on} \quad \Gamma_D \times [0, T], \qquad \mathbf{n} \cdot \mathbb{D}\nabla u = u_N \quad \text{on} \quad \Gamma_N \times [0, T]$$

and initial condition $u(\mathbf{x}, 0) = u_0(\mathbf{x})$ for $\mathbf{x} \in \Omega$, with all functions $u, f, u_D, u_N : \Omega \times [0, T] \to \mathbb{R}$ and $u_0 : \Omega \to \mathbb{R}$. In the following we consider, for simplicity, $\Gamma_N = \emptyset$ and $\Gamma_D = \partial\Omega$ but results can be extended to the other cases.

The right-hand side of (1) is a function $f \in L^2(\Omega)$ with $L^2(\Omega)$ the functional space of measurable functions on Ω that are square integrable in Ω, with norm $\|.\|_\Omega^2$ associated with the scalar product $(v, w)_\Omega = \int_\Omega v\, w$. Let $H^1(\Omega) = \{u \in L^2(\Omega),\ \nabla u \in L^2(\Omega)^2\}$ be the Hilbert space endowed with the semi-norm $|u|_{H^1(\Omega)} = \|\nabla u\|_\Omega$ and norm $\|u\|_{H^1(\Omega)}^2 = \|u\|_\Omega^2 + |u|_{H^1(\Omega)}^2$. We assume that $\partial\Omega$ is piece-wise $\mathcal{C}^1$, so that the trace operator $u \mapsto u_{|\partial\Omega}$ is continuous from $H^1(\Omega)$ to $L^2(\Gamma_D)$. We finally set $H_0^1(\Omega) = \{u \in H^1(\Omega),\ u_{|\partial\Omega} = 0\}$. Note that Ω is bounded, hence the $H^1(\Omega)$ seminorm is a norm on $H_0^1(\Omega)$. In the case we have $u_D \neq 0$, we set $H_D^1(\Omega) = \{u \in H^1(\Omega),\ u_{|\Gamma_D} = u_D\}$.

If the diffusion is isotropic (the same in any spatial direction) then $\mathbb{D} = c\,\mathbb{I}$, where c is the diffusion coefficient and $\mathbb{I}$ is here the 2×2 identity matrix. If the diffusion is anisotropic (variable with the spatial direction or even with the spatial position) then $\mathbb{D}$ is a symmetric positive definite matrix and its entries depend on the space coordinates. In these pages, the direction of the anisotropy is defined by a vector field $\mathbf{B} \neq \mathbf{0}$. We hence introduce the unit column vector $\mathbf{b} = (b_i)$ defined as $\mathbf{b} = \frac{\mathbf{B}}{|\mathbf{B}|}$, satisfying $|\mathbf{b}(\mathbf{x}, t)| = 1$ for all $(\mathbf{x}, t) \in \Omega \times [0, T]$, with $T > 0$. The symbol $\otimes$ will denote the vector tensor product, namely the matrix $\mathbf{b} \otimes \mathbf{b}$ has elements $(\mathbf{b} \otimes \mathbf{b})_{ij} = b_i\, b_j$. We thus consider the 2×2 matrix

$$\mathbb{D} = c_\parallel\, \mathbf{b} \otimes \mathbf{b} + c_\perp\, (\mathbb{I} - \mathbf{b} \otimes \mathbf{b}), \quad c_\parallel = \frac{1}{\epsilon}\, D_\parallel, \quad c_\perp = D_\perp, \quad 0 < \epsilon \ll 1,$$

with $D_\parallel$ and $D_\perp$ of comparable order of magnitude. The real $c_\parallel$ (resp., $c_\perp$) is the diffusion coefficient in the direction parallel (resp., perpendicular) to the vector $\mathbf{b}$, remaining in Ω. By decreasing the value of ϵ, we increase the difference between $c_\parallel$ and $c_\perp$.

To understand the expression of $\mathbb{D}$, let us assume for a moment that $\mathbf{n} = (\cos\theta\,, \sin\theta)$ and $\mathbf{b} = (-\sin\theta\,, \cos\theta)$ represent, respectively, the perpendicular and parallel unit vectors to the field $\mathbf{B}$. Matrix $\mathbb{D}$ being symmetric, it is diagonalisable by an orthogonal matrix R_θ,

namely

$$\mathbb{D} = R_\theta \Lambda R_\theta^\top, \qquad \Lambda = \begin{pmatrix} c_\perp & 0 \\ 0 & c_\parallel \end{pmatrix}, \qquad R_\theta = \begin{pmatrix} \cos\theta & -\sin\theta \\ \sin\theta & \cos\theta \end{pmatrix} = \begin{pmatrix} \mathbf{n}_x & \mathbf{b}_x \\ \mathbf{n}_y & \mathbf{b}_y \end{pmatrix}, \qquad R_\theta^\top R_\theta = \mathbb{I}.$$

Note that $\det(R_\theta) = 1$, with R_θ that rotates points in the xy-Cartesian plane counterclockwise through an angle θ about the origin of the Cartesian coordinate system in order to have the Cartesian axes aligned with $\mathbf{B}^\perp$ and $\mathbf{B}$. In other words, the unit vector $\mathbf{n}$ indicates the deviation of the Cartesian grid from being aligned with the magnetic field $\mathbf{B}$ and Λ contains the multiplying factors for the unit length in both directions.

Vectors $\mathbf{w} \in \mathbb{R}^2$ and gradients ∇u of scalar functions such as $u(\mathbf{x}, t)$, can be decomposed into a part parallel to the anisotropy direction $\mathbf{b}$ and a part perpendicular to it. In detail, a vector $\mathbf{w} \in \mathbb{R}^2$, can be written as $\mathbf{w} := \mathbf{w}_\parallel + \mathbf{w}_\perp$ with

$$\mathbf{w}_\parallel := (\mathbf{b} \cdot \mathbf{w})\, \mathbf{b} = (\mathbf{b} \otimes \mathbf{b})\, \mathbf{w}, \qquad \mathbf{w}_\perp := \mathbf{w} - \mathbf{w}_\parallel = (I - \mathbf{b} \otimes \mathbf{b})\, \mathbf{w}.$$

Analogously, for a scalar function $u(\mathbf{x}, t)$ we write $\nabla u = \nabla_\parallel u + \nabla_\perp u$ with

$$\nabla_\parallel u := (\mathbf{b} \cdot \nabla u)\, \mathbf{b}, \qquad \nabla_\perp u := (\mathbb{I} - \mathbf{b} \otimes \mathbf{b})\, \nabla u.$$

Let us consider the equation $\partial_t u - \nabla \cdot (\mathbb{D} \nabla u) = f$ and write it as follows:

$$\partial_t u - \nabla \cdot (\tfrac{1}{\epsilon} D_\parallel \mathbf{b} \otimes \mathbf{b} \nabla u) - \nabla \cdot (D_\perp (\mathbb{I} - \mathbf{b} \otimes \mathbf{b}) \nabla u) = f,$$

$$\partial_t u - \nabla \cdot (\tfrac{1}{\epsilon} D_\parallel \nabla_\parallel u) - \nabla \cdot (D_\perp \nabla_\perp u) = f,$$

$$\partial_t u - \nabla \cdot (c_\parallel \nabla_\parallel u) - \nabla \cdot (c_\perp \nabla_\perp u) = f.$$

The difficulty with the resolution of problem (1) is numerical, especially for small $0 < \epsilon \ll 1$. This occurs in a tokamak device (see,[18]), at the core of the plasma, where we have strong anisotropy in the diffusion coefficients, the parallel diffusion coefficient being much larger than the perpendicular one (e.g., $c_\parallel \approx 10^8\, c_\perp$). In the limit case (when $\epsilon = 0$), we would have (1) reduced to $-\nabla \cdot (D_\parallel \nabla_\parallel u) = 0$. Now, the field lines of $\mathbf{b}$ are concentric closed curves in the interior of Ω. By imposing periodic conditions in the parallel direction, we see that this reduced problem has an infinite number of solutions $u \in \mathcal{N}$, the Hilbert space $\{u \in H^1(\Omega),\ \nabla_\parallel u = \mathbf{0}\}$. All the functions in $\mathcal{N}$ are constant along the field lines of $\mathbf{b}$, in fact for $u \in \mathcal{N}$, the fact of verifying $\nabla_\parallel u = \mathbf{0}$ yields $\mathbf{b} \cdot \nabla u = 0$. At the discrete level, the system matrix is ill-conditioned due to the different order of magnitudes of the various terms appearing in (1). As a consequence standard numerical methods, adopted for the resolution of the corresponding linear system, may yield to high approximation errors. Ill-conditioning is a key difficulty for full 3D simulations of plasma discharges and it is an active area of research.

2.1 | Deriving a one-dimensional reduced problem

In plasma applications, because of the strong anisotropy, the transport of the heat and of other quantities concerns mainly the radial direction. Hence, in specialized MHD codes (such as `NICE`[19], `CRONOS`[20], for example), when it comes to developing numerical approaches

for simulating plasma evolution on the time scales of heat and current diffusion, some variables are (time dependent) one-dimensional radial profiles, corresponding with the average of the physical quantities over an infinitesimal volume around a flux surface of given radial position. This allows for a simplification in the code writing and reduces CPU time and memory requirements, especially when there are many equations to consider, as it occurs with the simulation and control of a tokamak plasma discharge. Reduced models can be discretized by suitable finite difference schemes, thus avoiding numerical drawbacks generally associated with a FE approach on the full problem, such as, for example, the numerical diffusion here considered. It has to be said that the definition of such reduced models by the averaging technique (as explained in Chap. 5 in [21] and Chap. 6 in [1]) in more general non-linear multiscale configurations is a delicate and difficult step (in MHD applications, see an example in [22,23,24]).

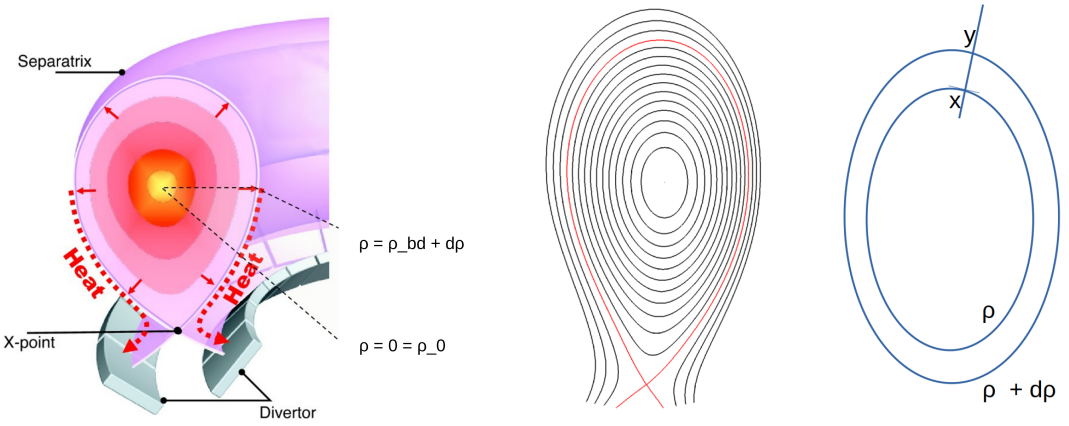

Figure 1 (Left, courtesy C. Paz-Soldan) A simplified representation of the flux surfaces (contours of equal magnetic flux) and heat transport direction in a tokamak. Note that for $\rho = \rho_{bd} + d\rho$ we have the separatrix contour which is not smooth in the X-point. Therefore, we set $\rho_\partial = \rho_{bd}$ in order to exclude the separatrix contour. (Center) The magnetic poloidal flux contours ($\psi = \text{const}$) for a standard plasma equilibrium in a tokamak (see [1]). Two of such contours, indexed by ρ and $\rho + d\rho$ (right). The normal line to the contour ρ cutting through $\mathbf{x}$ intersects the contour $\rho + d\rho$ in a point $\mathbf{y}$.

In this section, we provide a reduced model in a simplified situation, that is with one scalar field (the temperature u) solution of a linear equation in a coordinate system with velocity $\mathbf{v}_\rho = \mathbf{0}$, with the purpose of commenting on some obtained results. The considered reduced model is obtained from (1) by averaging quantities over the two-dimensional domain Ω and applying a two-dimensional form of the coarea formula (see Thm 3.2.12 in [25] for the general form). In MHD computations, the coarea would be applied in its three-dimensional form to the domain $\tilde{\Omega} = \Omega \times [0, 2\pi]$ (in cylindrical coordinates $((R, Z), \phi)$) which is the interior of a closed magnetic surface (enclosed by the separatrix, which is not smooth).

Proposition 1. Let Ω be a Jordan domain and $g : \Omega \to [\rho_0, \rho_\partial]$ a $\mathcal{C}^1$, a.e. invertible transformation in a new coordinate system. Let $u : \Omega \to \mathbb{R}$ be a continuous function. Then the weight of u on Ω can be written as

$$\int_\Omega u(\mathbf{x})\, dS = \int_{\rho_0}^{\rho_\partial} \left(\oint_C \frac{u(\mathbf{x})\, ds}{|\nabla g(\mathbf{x})|} \right) d\rho, \tag{2}$$

where C is the closed field line indexed by ρ and s is the curvilinear abscissa on C.

Proof. We first introduce $g : \Omega \to [\rho_0, \rho_\partial]$, a smooth (i.e., $\mathcal{C}^1$), invertible a.e. in Ω (i.e., $\nabla g(\mathbf{x}) \neq \mathbf{0}$ almost everywhere in Ω) coordinate transformation on Ω, aligned with $\mathbf{b}$, that is ρ is the coordinate indexing the (closed) contours of $\mathbf{b}$ and varies in the interval $[\rho_0, \rho_\partial]$. Let $\mathbf{x} \in \Omega$ be such that $\nabla g(\mathbf{x}) \neq \mathbf{0}$ and $g(\mathbf{x}) = \rho$. We slightly increase ρ of a quantity $d\rho$ and obtain the nearby contour indexed by $\rho + d\rho$ (see Fig. 1). The line cutting through $\mathbf{x}$, perpendicularly to the ρ-contour, intersects the nearby contour in a point $\mathbf{y}$. We thus have, $g(\mathbf{y}) = \rho + d\rho$ and obtain the following estimate (by first order of approximation)

$$d\rho = g(\mathbf{y}) - g(\mathbf{x}) \approx \nabla g(\mathbf{x}) \cdot (\mathbf{y} - \mathbf{x}).$$

Note that $\nabla g(\mathbf{x}) \perp C$ by construction, with $C = \{\mathbf{p} \in \Omega,\, g(\mathbf{p}) = \rho\}$. Moreover, $(\mathbf{y}-\mathbf{x}) \perp C$ by construction too, since $\mathbf{y}$ is the intersection point of the contour indexed by $\rho + d\rho$ with the line cutting through $\mathbf{x}$ perpendicularly to C. Hence, $\nabla g(\mathbf{x}) \parallel (\mathbf{y} - \mathbf{x})$, with the same direction, since $d\rho > 0$. So, $\nabla g(\mathbf{x})$ and $(\mathbf{y} - \mathbf{x})$ lie on the same line, and we can write

$$d\rho \approx \nabla g(\mathbf{x}) \cdot (\mathbf{y} - \mathbf{x}) = |\nabla g(\mathbf{x})|\, |(\mathbf{y} - \mathbf{x})| \qquad \Longrightarrow \qquad |(\mathbf{y} - \mathbf{x})| \approx \frac{d\rho}{|\nabla g(\mathbf{x})|}\,.$$

Now, we take a line element ds centered at $\mathbf{x}$ on the contour C indexed by ρ and consider the elemental surface $dS = |(\mathbf{y}-\mathbf{x})|\, ds$. Being u continuous and dS very small, the value of u in dS does not change significantly. We can assume that u is constant on dS, equal to $u(\mathbf{x})$. Therefore,

$$u(\mathbf{x})\, dS = u(\mathbf{x})\, |(\mathbf{y} - \mathbf{x})|\, ds = \frac{u(\mathbf{x})}{|\nabla g(\mathbf{x})|}\, d\rho\, ds.$$

We let $\mathbf{x}$ move along C and by summing up all the contributions $u(\mathbf{x})\, dS$, we have the integral of u on the surface enclosed between the contours indexed by ρ and $\rho + d\rho$, namely

$$\int_{[0,2\pi]\times[\rho,\rho+d\rho]} u(\mathbf{x})\, dS = \oint_C \frac{u(\mathbf{x})}{|\nabla g(\mathbf{x})|}\, d\rho\, ds.$$

The integral of u on Ω is obtained by summing up with respect to ρ, that is

$$\int_\Omega u(\mathbf{x})\, dS = \int_{\rho_0}^{\rho_\partial} \left(\oint_C \frac{u(\mathbf{x})}{|\nabla g(\mathbf{x})|}\, d\rho\, ds \right) = \int_{\rho_0}^{\rho_\partial} \left(\oint_C \frac{u(\mathbf{x})}{|\nabla g(\mathbf{x})|}\, ds \right) d\rho\,,$$

which is the desired formula. □

When the anisotropy is strong, we wish to work with quantities that only depend on the coordinate ρ and on time t, we introduce the average $\langle u \rangle = \frac{\partial}{\partial S} \left(\int_S u\, dS \right)$ of an arbitrary quantity u over the domain S (see [21] for more details). When the functions u is constant on

each magnetic surface, by differentiating with respect to ρ the coarea formula (where we have identified g with ρ), we have

$$\frac{\partial}{\partial \rho}\left(\int_S u\, dS\right) = \oint_C u\, \frac{ds}{|\nabla \rho|}\,.$$

Noting that $\frac{\partial}{\partial \rho}(.) = \frac{\partial S}{\partial \rho}\frac{\partial}{\partial S}(.) = \Theta_\rho \frac{\partial}{\partial S}(.)$, we can write

$$\frac{\partial}{\partial \rho}\left(\int_S u\, dS\right) = \Theta_\rho \langle u\rangle\,, \qquad \langle u\rangle := \frac{1}{\Theta_\rho}\left(\oint_C u\, \frac{ds}{|\nabla \rho|}\right), \qquad \Theta_\rho := \oint_C \frac{ds}{|\nabla \rho|}\,.$$

The magnetic field and flux surfaces evolve and change in time. Under the assumption, for simplicity, of zero coordinate velocity ($\mathbf{v}_\rho = \mathbf{0}$), we have $\partial_t \langle u\rangle = \langle \partial_t u\rangle$. The average of the two-dimensional divergence of a vector $\mathbf{w}$ is

$$\begin{aligned}\langle \nabla\cdot\mathbf{w}\rangle &= \tfrac{\partial}{\partial S}\left(\textstyle\int_S \nabla\cdot\mathbf{w}\, dS\right) = \tfrac{\partial}{\partial S}\left(\oint_C \mathbf{w}\cdot\mathbf{n}\, ds\right)\\ &= \tfrac{\partial}{\partial S}\left(\oint_C \mathbf{w}\cdot\tfrac{\nabla\rho}{|\nabla\rho|}\, ds\right) = \tfrac{\partial}{\partial S}\left(\,\Theta_\rho\,\langle \mathbf{w}\cdot\nabla\rho\rangle\,\right) = \tfrac{1}{\Theta_\rho}\tfrac{\partial}{\partial \rho}\left(\,\Theta_\rho\,\langle \mathbf{w}\cdot\nabla\rho\rangle\,\right).\end{aligned}$$

Hence, by averaging (1) over each magnetic ρ-contour we obtain

$$\langle\, \partial_t u\,\rangle - \langle\, \nabla\cdot(\mathbb{D}\,\nabla u)\,\rangle = \langle\, f\rangle$$

$$\partial_t \langle u\rangle - \tfrac{1}{\Theta_\rho}\,\partial_\rho\left(\,\Theta_\rho\,\langle \mathbb{D}\,\nabla u\cdot\nabla\rho\rangle\,\right) = \langle f\rangle.$$

The functions u and f are supposed to be constant on each ρ-surface (i.e., $\partial_\theta u = 0$). Hence, we set $\langle u\rangle = \tilde{u}$ and $\langle \partial_\rho u\rangle = \partial_\rho\langle u\rangle$ holds true. We have $\mathbb{D}\,\nabla u = c_\parallel\,\frac{1}{\rho}\,\partial_\theta u\,\mathbf{e}_\theta + c_\perp\,\partial_\rho u\,\mathbf{e}_\rho = c_\perp\,\partial_\rho u\,\mathbf{e}_\rho$ with $\mathbf{e}_\rho = \frac{\nabla\rho}{|\nabla\rho|}$ and we thus get

$$\mathbb{D}\,\nabla u\cdot\nabla\rho = c_\perp\,\partial_\rho u\,|\,\nabla\rho\,|\,, \qquad \langle \mathbb{D}\,\nabla u\cdot\nabla\rho\rangle = c_\perp\,\partial_\rho\tilde{u}\,\langle\,|\nabla\rho|\rangle\,.$$

It finally results

$$\partial_t\,\tilde{u} - \frac{1}{\Theta_\rho}\,\partial_\rho\left(\,c_\perp\,\Theta_\rho\,C_1(t,\rho)\,\partial_\rho\tilde{u}\,\right) = \tilde{f}, \qquad \text{with} \qquad C_1(t,\rho) = \langle\,|\,\nabla\rho\,|\,\rangle\,.$$

So, if $\tilde{u}(t,\rho)$ denotes the average of $u(t,\theta,\rho)$ in the parallel direction (similarly for $\tilde{f}$) equation (1) becomes

$$\partial_t\,\tilde{u} - \frac{1}{\Theta_\rho}\,\partial_\rho(c_\perp\,\Theta_\rho\,C_1(t,\rho)\,\partial_\rho\,\tilde{u}) = \tilde{f}\,, \qquad \forall\,(\rho,t)\in[\rho_0,\rho_\partial]\times[0,T], \qquad T>0 \tag{3}$$

with $\partial_\rho\tilde{u}(\rho_0,t) = 0$, $\tilde{u}(\rho_\partial,t) = \langle u_D\rangle$ and $\tilde{u}(\rho,0) = \langle u_0\rangle$. Here, $C_1(t,\rho)$ is a geometric coefficient, and $\Theta_\rho := \partial_\rho S(\rho)$ with $S(\rho)$ the surface bounded by the ρ-contour. So, if the temperature u is nearly constant on flux contour we can do surface averages and work with equation (3) for a function $\tilde{u}$ dependent only on the surface coordinate ρ and the time t.

Remark 1. In plasma applications, a reduced model as (3) is valid in the core but it is no more useful when approaching to the plasma boundary. In the core, (3) degenerates for $\rho_0 = 0$. Indeed, $S(0) = 0$ and $\Theta_\rho(0) = 0$ and $\tilde{u}$ cannot be defined. Comparing (1) to (3), we have passed from a two-dimensional domain Ω with boundary $\partial\Omega$ to an interval $[\rho_0,\rho_\partial]$ having two extremities. It is reasonable to keep the Dirichlet boundary condition at $\{\rho_\partial\}\times[0,T]$ and adopt a homogeneous Neumann condition $\partial_\rho\tilde{u} = 0$ at $\{\rho_0\}\times[0,T]$ when $\rho_0 = 0$.

Example 1. (Reduced problem associated with (1) over a disk) Let $\Omega = D(\mathbf{0}, R_\partial)$ and $D(\mathbf{0}, R)$ denoting the disk of center $\mathbf{0}$ and radius R. In this example, $g : \Omega \to [\rho_0, \rho_\partial]$ is defined as $g(\mathbf{x}) = \sqrt{x^2 + y^2} = R(= \rho)$. Here, $d\rho = dR$, $ds = R\, d\theta$ and $\nabla g(\mathbf{x}) = (\frac{x}{R}, \frac{y}{R})$ (defined for $R \neq 0$) and $|\nabla g(\mathbf{x})| = 1$. By using the coarea formula we get

$$\int_0^{R_\partial} \left(\oint_C \frac{u(\mathbf{x})}{1} R\, d\theta \right) dR = \int_0^{R_\partial} \left(\int_0^{2\pi} u(\mathbf{x})\, d\theta \right) R\, dR$$

which is the integral $\int_\Omega u(\mathbf{x})\, dS$ rewritten in polar coordinates (R, θ). It has to be noted that for a Jordan domain

$$\Theta_\rho\, C_1(t, \rho) = \oint_C |\nabla \rho| \frac{ds}{|\nabla \rho|} = \oint_C ds = P(\rho)$$

with $P(\rho)$ the perimeter of $S(\rho)$. For the considered Ω, we have $\rho = R$, $C_1(t, \rho) = 1$, $S(\rho) = \pi R^2$ and $\Theta_\rho = 2\pi R(= \partial_\rho S(\rho))$. The model equation (3) becomes

$$\partial_t \tilde{u} - \frac{1}{R} \partial_R (c_\perp R \partial_R \tilde{u}) = \tilde{f},$$

which yields

$$\partial_t \tilde{u} - \frac{c_\perp}{R} \partial_R \tilde{u} - c_\perp \partial^2_{RR} \tilde{u} = \tilde{f}, \qquad \forall (R, t) \in]0, R_\partial] \times [0, T], \qquad T > 0. \tag{4}$$

If $c_\perp = 0$ and $\tilde{f} = 0$, the solution of problem (3) is $\tilde{u} = \tilde{u}_0$ in $[0, R_\partial] \times [0, T]$. If $c_\perp \neq 0$, equation (4) can be discretized, for example, by the θ-method in time and centered finite differences or finite volumes in space, in order to have an approximated solution (see, [26]).

In the present case, we are interested in analysing the numerical diffusion associated with a C1 FE discretization of the full problem (1) for the heat transport. In plasma applications, FE discretizations are indeed used to solve the force equilibrium problem (e.g., the Grad-Shafranov equation). This allows to compute the magnetic flux distribution in Ω, thus the coordinate system aligned with the anisotropy that, in the core of the plasma, makes the reduction procedure possible.

2.2 | The weak form of the model problem

To derive the variational formulation of the full considered problem, we take the product of (1) with a test function v, we integrate over the domain Ω and use the Stokes's theorem for the term containing the divergence. We thus obtain : for each $t \in [0, T]$, find a function $u(t) \in H^1(\Omega)$ such that $u(t) - u_D(t) \in H^1_0(\Omega)$ and

$$d_t \int_\Omega u\, v + \int_\Omega \mathbb{D} \nabla u \cdot \nabla v = \int_\Omega f\, v, \qquad \forall v \in H^1_0(\Omega). \tag{5}$$

Note that Ω is bounded, therefore the $H^1(\Omega)$ seminorm is a norm on $H^1_0(\Omega)$. In the rest of the paper, we assume that $D_\parallel$, $D_\perp \in L^\infty(\Omega)$, both taking values, for almost all $x \in \Omega$, in the interval $[D_0, D_1]$, with $D_0 > 0$.

Proposition 2. Let $\mathrm{mes}\,(\Gamma_D) > 0$ and $\epsilon > 0$ so that the coefficients $c_\parallel$, $c_\perp$, are bounded and positive. Then, for $f \in L^2((0, T); L^2(\Omega))$ and $u_0 \in L^2(\Omega)$, problem (5) admits a unique solution $u \in L^2((0, T); H^1_D(\Omega)) \cap \mathcal{C}^0((0, T); L^2(\Omega))$, such that $u(0) = u_0$.

Proof. Let us assume that $u_D = 0$. Since $c_\parallel$ and $c_\perp$ are supposed bounded and positive, there exist $c_0, c_1 \in \mathbb{R}$ such that $0 < c_0 \leq c_\perp < c_\parallel \leq c_1$ for almost all $x \in \Omega$. The bilinear form of problem (5) is coercive on $\mathcal{X} = H_0^1(\Omega)$, namely, there is a positive constant $\alpha > 0$ such that $(\mathbb{D}\nabla u, \nabla u) \geq \alpha \, ||u||_{\mathcal{X}}^2$ for all $u \in \mathcal{X}$. Indeed,

$$\begin{aligned}
(\mathbb{D}\nabla u, \nabla u) &= c_\parallel \, (\mathbf{b} \otimes \mathbf{b} \nabla u, \nabla u) + c_\perp ((I - \mathbf{b} \otimes \mathbf{b}) \nabla u, \nabla u) \\
&= c_\parallel \int_\Omega |\mathbf{b}^\top \cdot \nabla u|^2 + c_\perp \, ||\nabla_\perp u||_{L^2}^2 \\
&= c_\parallel \, \|\nabla_\parallel u\|_{L^2}^2 + c_\perp \, ||\nabla_\perp u||_{L^2}^2 \\
&\geq c_0 \, (\, \|\nabla_\parallel u\|_{L^2}^2 + ||\nabla_\perp u||_{L^2}^2 \,) = \alpha ||u||_{\mathcal{X}}^2
\end{aligned}$$

with $\alpha = c_0 > 0$, the H^1 seminorm being a norm on $\mathcal{X}$ and $\nabla u = \nabla_\parallel u + \nabla_\perp u$.

Continuity holds when there exists $\gamma > 0$ such that $|(\mathbb{D}\nabla u, \nabla v)| \leq \gamma \, ||u||_{\mathcal{X}} \, ||v||_{\mathcal{X}}$ for all $u, v \in \mathcal{X}$. Indeed, we have

$$\begin{aligned}
|(\mathbb{D}\nabla u, \nabla v)| &\leq c_\parallel |(\mathbf{b} \otimes \mathbf{b} \nabla u, \nabla v)| + c_\perp |((I - \mathbf{b} \otimes \mathbf{b}) \nabla u, \nabla v)| \\
&\leq c_\parallel \, ||\nabla_\parallel u||_{L^2} \, ||\nabla v||_{L^2} + c_\perp \, ||\nabla_\perp u||_{L^2} ||\nabla v||_{L^2} \\
&\leq c_1 \, (\, \|\nabla_\parallel u\|_{L^2} ||\nabla v||_{L^2} + ||\nabla_\perp u||_{L^2} ||\nabla v||_{L^2} \,) \leq \gamma \, ||u||_{\mathcal{X}} \, ||v||_{\mathcal{X}}
\end{aligned}$$

with $\gamma = 2\, c_1 > 0$. Under the considered conditions on u_0 and f, together with the properties of the bilinear form, problem (5) admits a unique solution u for $u_D = 0$ (see, e.g., [27]). When $u_D \neq 0$, a similar proof is carried out working with $u - u_D \in \mathcal{X}$ instead of u. □

The following proposition states that the solution u of problem (5) is stable in time, namely, for any $t \in [0, T]$, its energy $E(t) = \int_\Omega u^2(t)$ is bounded.

Proposition 3. For any $t \in [0, T]$, it holds $E(t) \leq e^{-\nu\, t} E(0) + \frac{1}{\nu} \int_0^t e^{\nu\,(s-t)} \, ||f(s)||_{L^2}^2$ with the constant $\nu > 0$ independent of t.

Proof. Once again, we set $u_D = 0$. Let us consider (1) multiplied by $u(t)$ and integrated in space over Ω. We obtain

$$\begin{aligned}
\textstyle\int_\Omega (\partial_t u) \, u - \int_\Omega \nabla \cdot (\mathbb{D} \nabla u) \, u = \int_\Omega f \, u \, , \\
\tfrac{1}{2} \textstyle\int_\Omega \partial_t (u^2) + \int_\Omega \mathbb{D} \nabla u \cdot \nabla u = \int_\Omega f \, u \, , \\
\tfrac{1}{2} \, d_t \, E(t) + \textstyle\int_\Omega \mathbb{D} \nabla u \cdot \nabla u = \int_\Omega f \, u \, ,
\end{aligned}$$

by relying on the integration by parts and on the fact that we can interchange time differentiation and space integration in the first term on the left-hand side. By using the Cauchy-Schwarz inequality, we have $\int_\Omega f \, u \leq (\int_\Omega f^2)^{\frac{1}{2}} \, (\int_\Omega u^2)^{\frac{1}{2}}$. Let $E_f(t) = \int_\Omega f^2(t)$ be an energy for the function f, we get $\int_\Omega f \, u \leq (E_f(t))^{\frac{1}{2}} \, (E(t))^{\frac{1}{2}}$ and thus

$$d_t \, E(t) + 2 \int_\Omega \mathbb{D} \nabla u \cdot \nabla u \leq 2 \, (E_f(t))^{\frac{1}{2}} \, (E(t))^{\frac{1}{2}} .$$

Due to the Poincaré inequality, we have that $\int_\Omega \mathbb{D} \nabla u \cdot \nabla u \geq \nu \int_\Omega u^2$ with $\nu = c_\perp / (C_\Omega)^2$, being C_Ω the Poincaré constant of Ω. It results

$$d_t \, E(t) + 2 \, \nu \, E(t) \;\leq\; 2 \, (E_f(t))^{\frac{1}{2}} \, (E(t))^{\frac{1}{2}} \;\leq\; \nu \, E(t) + \frac{1}{\nu} \, E_f(t) \tag{6}$$

by involving the Young inequality $a\,b \leq \frac{\epsilon}{2}\,a^2 + \frac{1}{2\epsilon}b^2$ for all $a, b \in \mathbb{R}$ and any $\epsilon > 0$ (here, we can choose $\epsilon = \nu$). Inequality (6) yields $d_t\,E(t) + \nu\,E(t) \leq \frac{1}{\nu}\,E_f(t)$ that, multiplied by $e^{\nu\,t}$ on each side, gives

$$d_t\left(e^{\nu\,t}E(t)\right) \leq \frac{e^{\nu\,t}}{\nu}\,E_f(t)$$

since $d_t\left(e^{\nu\,t}E(t)\right) = \nu\,e^{\nu\,t}\,E(t) + e^{\nu\,t}\,d_t\,E(t)$. We integrate in time, from 0 to $t \leq T$ and we obtain

$$e^{\nu\,t}E(t) - E(0) \leq \frac{1}{\nu}\int_0^t e^{\nu\,s}\,E_f(s)\,ds, \qquad E(t) \leq e^{-\nu\,t}E(0) + \frac{1}{\nu}\int_0^t e^{\nu\,(s-t)}\,E_f(s)\,,$$

thus the result. For $f = 0$, the inequality states that $E(t)$ decreases exponentially in time. □

The well-posedness stated above for problem (1), can be proven also for the discrete problem we are going to construct in the following sections, by relying on similar reasoning and on the discrete form of the (Cauchy-Schwarz, Young, ...) inequalities.

3 | SEMI-DISCRETE PROBLEM BY C1 FINITE ELEMENTS

The variational problem (5) is discretized by a conforming finite element method (FEM) to get a system of ordinary differential equations (ODEs). To this end, we assume that the original domain Ω is replaced by a mesh τ_h, namely, a finite set of non-overlapping (quadrangular or triangular) elements, having uniform size h, such that $\bar{\Omega} \approx \bar{\Omega}_h = \cup_{T\in\tau_h} T$. The discretization τ_h is geometrically conforming, i.e., the intersection between two distinct elements T, $T' \in \tau_h$ is either the empty set or a common vertex or a common side. The discrete problem associated with (5) reads: for each $t \in [0, T]$, find $u_h(t) \in \mathcal{X}_h$ with $u_h(t) - u_{hD}(t) \in \mathcal{X}_{h,0}$ such that $u_h(\mathbf{x}, 0) = u_{0,h}(\mathbf{x})$ for $\mathbf{x} \in \Omega_h$ and

$$d_t \int_{\Omega_h} u_h\,v_h + \int_{\Omega_h} \mathbb{D}\,\nabla u_h \cdot \nabla v_h = \int_{\Omega_h} f_h\,v_h, \qquad \forall v_h \in \mathcal{X}_{h,0}, \tag{7}$$

being $u_{0,h} = \mathcal{I}_h u_0$ a reconstruction of u_0 in $\mathcal{X}_h$. Similarly, we set $f_h = \mathcal{I}_h f$ and $u_{hD}(t) = \mathcal{I}_h u_D(t)$, respectively. By arguments similar to those used in the proof of Proposition 2, we can show that Problem (7) has a unique solution $u_h(t) \in \mathcal{X}_h$ for each $t \in [0, T]$ (see also, e.g.,[27]). We construct the discrete space $\mathcal{X}_h$ in the case where either reduced Hsieh-Clough-Tocher (rHCT) FEs on a triangular grid or Hermite Bézier (HB) FEs on a quadrangular grid are adopted, and we set $\mathcal{X}_{h,0} = \mathcal{X}_h \cap H_0^1(\Omega)$ and $\mathcal{X}_{h,D} = \mathcal{X}_h \cap H_D^1(\Omega)$.

△ Let us represent $\bar{\Omega}_h$ by a mesh τ_h with triangles having straight edges. To achieve C^1 regularity for the solution u_h of problem (7) in Ω_h, we consider the discrete space $\mathcal{X}_h = \{v \in C^1(\Omega_h),\, v_{|T} \in \mathcal{P}_{loc}(T),\, \forall\, T \in \tau_h\}$, with $\mathcal{P}_{loc}(T)$ given in Definition 1 of[13]. We recall that, locally, the rHCT finite element is the triple $(T, \mathcal{P}_{loc}(T), \Sigma(T))$ where T denotes a triangle of the mesh τ_h, $\mathcal{P}_{loc}(T)$ the local space of functions defined on that triangle and $\Sigma(T)$ a set of unisolvent degrees of freedom for the functions in the local space (see[28]). Any triangle $T = [V_1, V_2, V_3]$ of the mesh τ_h is cut into three triangles $\mathtt{B}_i$: each $\mathtt{B}_i = [G, V_m, V_\ell]$ having vertices in V_m, V_ℓ with $m, \ell \in \{1, 2, 3\} \setminus \{i\}$ and at the barycenter G of the triangle T. We can thus reconstruct the height $u_h(V_i)$ of the function u_h at the three vertices V_i of T and the tangent plane to the surface u_h at the vertices V_i, as generated by $\partial_x u_h(V_i), \partial_y u_h(V_i)$. In the

following, we denote by $\{\phi_i\}_{i=1,3N_h}$ the basis of $\mathcal{X}_h$ in duality with the degrees of freedom associated with the N_h nodes of τ_h and we refer to [29] for its detailed construction.

- Another way to achieve C^1 regularity in Ω_h is to rely on isoparametric bi-cubic Hermite Bézier FEs over curved quadrangular elements in the physical space, as stated in [10]. Meshes with curved elements allow to analyse the accuracy of the proposed approach when the geometrical discretization is aligned with the vector field $\mathbf{b}$ appearing in the diffusion tensor $\mathbb{D}$. We thus seek for u_h solution of problem (7) in Ω_h in the discrete space $\mathcal{X}_h = \{z \in C^1(\Omega_h),\, z_{|Q_e} \circ F_e^{-1} \in \mathcal{P}_{loc}(\hat{Q}),\, \forall\, Q_e \in \tau_H\}$ with $\mathcal{P}_{loc}(\hat{Q})$ defined in Definition 3 of [13]. Note that with these FEs we simultaneously build a $\mathcal{C}^1$ representation Ω_h of the domain Ω and of the solution u_h of (7). We denote by $\{\psi_k\}_{k=1,4N_h}$ the basis of $\mathcal{X}_h$ in duality with the dofs associated with vertices $V_i \in \tau_h$.

In order to treat correctly the term $\int_{\Omega_h} \mathbb{D}\nabla u_h \cdot \nabla v_h$ in (7) when strong anisotropic effects occur, we may rely on a coordinate system aligned with $\mathbf{B}$ (see [6]). This is possible within an isoparametric FE approach such as with the HB FEs. With rHCT FEs we can proceed as follows. We work in cylindrical coordinates (R, ϕ, Z) and we are looking for an axisymmetric solution, namely a field u with $\partial_\phi u = 0$. The magnetic induction $\mathbf{B}$, at the origin of the anisotropy, is solenoidal thus it can be written as $\nabla \times \mathbf{A}$ with $\mathbf{A} = (A_R, A_\phi, A_Z)$ the magnetic vector potential. Using axisymmetry, we have

$$\mathbf{B} = \nabla \times (A_\phi\, \mathbf{e}_\phi) + (\partial_Z A_R - \partial_R A_Z)\, \mathbf{e}_\phi$$

with $\mathbf{e}_\phi$ the unit vector in the ϕ (toroidal) direction. We thus introduce the poloidal flux function $\psi(R, Z) = R\, A_\phi$ and the toroidal field function $f(R, Z) = R\,(\partial_Z A_R - \partial_R A_Z)$. Hence,

$$\mathbf{B} = \frac{1}{R}\nabla\psi(R, Z) \times \mathbf{e}_\phi + \frac{f(R, Z)}{R}\, \mathbf{e}_\phi = \mathbf{B}_{pol} + \mathbf{B}_{tor}. \tag{8}$$

This is a general result for axisymmetric systems that the magnetic field can always be expressed as the sum of poloidal and toroidal terms involving two scalar functions, namely ψ and f. The contours $\psi(R, Z) = \text{const}$ are closed within the plasma region, forming nested toroidal surfaces. The magnetic field $\mathbf{B}$ lies on these $\psi(R, Z) = \text{const}$ surfaces since it holds $\mathbf{B} \cdot \nabla\psi = 0$. In a poloidal section ($\phi = \text{const}$), that we have called Ω, close to the magnetic axis, the field lines are circular, and become vertically elongated approaching the separatrix (which is the longest closed field line passing by the X-point, the red line in Fig. 1, left). We adopt an axisymmetric magnetic flux coordinate system (ρ, ϕ, θ) where $\rho(\psi)$ is a magnetic flux coordinate, θ is a poloidal angle (that goes the short way around the torus), and ϕ is the standard toroidal angle of the cylindrial coordinate system. At any given time we have the flux coordinates (ρ, ϕ, θ) and the inverse representation $\mathbf{x} = (R, \phi, Z)$, since the magnetic field and flux surfaces described by ψ evolve and change in time. However, we suppose that the coordinate velocity $\mathbf{v}_\rho$ is negligible ($\mathbf{v}_\rho = \mathbf{0}$), that is $\partial_t \mathbf{x} \approx \mathbf{0}$ so that $(\partial_t u)_{|(\rho,\phi,\theta)} = (\partial_t u)_{|\mathbf{x}}$, for any axisymmetric function u. In equation (5), this yields indeed $\int_\Omega \partial_t u\, v = d_t \int_\Omega u\, v$. Let $\Phi : (\rho, \theta) \mapsto (R, Z)$ be the isomorphism between the two reference systems in the poloidal section. The Jacobian of the transformation Φ is $J = (\partial_\rho R\, \partial_\theta Z - \partial_\theta R\, \partial_\rho Z)$. We set an orthogonal coordinate

reference system $(\mathbf{e}_\rho, \mathbf{e}_\theta)$ in the poloidal section Ω so that

$$\mathbf{e}_\theta = \mathbf{b}\,, \qquad \mathbf{e}_\theta \cdot \mathbf{e}_\rho = 0\,, \qquad \mathbf{e}_\rho = \frac{\nabla\psi}{|\nabla\psi|}\,.$$

with $\mathbf{b} = \mathbf{B}_{pol}/|\mathbf{B}_{pol}|$. For the term in $\mathbb{D}$ appearing in (5), we have

$$\int_{\Omega_h} \mathbb{D}\nabla u_h \cdot \nabla v_h = \sum_{T\in\tau_h} \int_T [\delta c\, \nabla_\parallel u_h \cdot \nabla_\parallel v_h + c_\perp \nabla u_h \cdot \nabla v_h]$$

with $\delta c = c_\parallel - c_\perp$ and contributions on $T \in \tau_h$ evaluated by a quadrature formula. For example,

$$\int_T c_\perp \nabla u_h \cdot \nabla v_h = \sum_{\mathbf{x}_q \in T} c_\perp\, \omega_q\, (\nabla u_h)_{|\mathbf{x}_q} \cdot (\nabla v_h)_{|\mathbf{x}_q}\,,$$

with ω_q, $\mathbf{x}_q$, the Gauss quadrature weights and points, respectively. In particular, taking advantage of an aligned mesh, we obtain

$$\int_T \delta c\, \nabla_\parallel u_h \cdot \nabla_\parallel v_h = \int_T \delta c\, (\mathbf{b}\cdot\nabla u_h)(\mathbf{b}\cdot\nabla v_h) = \int_{\Phi^{-1}(T)} \delta c\, \partial_\theta u_h\, \partial_\theta v_h\, \frac{R^2}{|\nabla\psi|^2}\, J\, d\rho\, d\theta$$

with $\nabla\psi = \partial_\rho\psi\, \nabla\rho$, $\nabla\rho = \frac{1}{J}(\partial_\theta Z, 0, -\partial_\theta R)^\top$ and $\Phi^{-1}(T)$ denotes the T domain in the (ρ,θ) reference system.

Example 2. (Solov'ev equilibrium) We consider a well-known exact analytic solution of the Grad-Shafranov (GS) equation in the plasma domain, the Solov'ev equilibrium, which assumes the plasma pressure p and the poloidal current flux f to be linear functions of the poloidal flux function ψ (see, e.g.,[6]). In the plasma domain, the GS equation for ψ in the (R, Z) coordinates can be written as follows

$$R\,\partial_R\Big(\frac{1}{R}\partial_R\psi\Big) + \partial_{ZZ}\psi = -\,\mu_0\, R^2\, d_\psi p - \frac{1}{2}\, d_\psi f^2$$

with μ_0 the magnetic permeability of the vacuum. The Solov'ev equilibrium is computed by assuming that $d_\psi p = -\frac{c_1}{\mu_0}$ and $\frac{1}{2}\, d_\psi f^2 = -c_2\, R_0^2$, with c_1, c_2 two real constants (and $c_1 + c_2 \neq 0$). In this case, the magnetic surfaces correspond with manifolds of constant values for ψ given by

$$\psi(R,Z) = \frac{1}{2}[\, c_0\, a^2\, R_0^2 + (c_2\, R_0^2 + c_3\, R^2)\, Z^2 + \frac{1}{4}\,(c_1 - c_3)(R^2 - R_0^2)^2\,],$$

with c_0, c_3 arbitrary constants, and a, R_0, respectively, the small and large radius of the tokamak. A useful choice for tokamak application is to set $c_0 = 1$, $c_1 = c_2 = -1$, $c_3 = 0$, that yields

$$\psi(R,Z) = \frac{1}{2} R_0^2 \left(a^2 - \, Z^2 - \frac{(R^2 - R_0^2)^2}{4\, R_0^2}\right)$$

which can be solved analytically to give the explicit form of the contour of ψ on (R, Z) plane. We thus work in Ω bounded externally by the contour $\psi = 0$ with the plasma axis in $(R_c, 0)$, being $R_c > 0$, namely the boundary of Ω is

$$\partial\Omega = \Big\{ (R,Z) = (R_0\,(R_c + 2a\,\cos\theta)^{\frac{1}{2}}\ ,\ aR_0\,\sin\theta\,)\,,\ \theta \in [0, 2\pi] \Big\}\,.$$

In order to specify the transformation Φ in the case of the Solov'ev equilibrium, we set for simplicity $a = 0.5$ and $R_0 = 1$. The Solov'ev equilibrium is described by $\psi(R,Z) = \frac{1}{8}(1 - 4Z^2 - (R^2-1)^2)$ and we have

$$(R,Z) = \Phi(\rho,\theta) = ((R_c + \rho^{\frac{1}{2}}\cos\theta)^{\frac{1}{2}}, \frac{1}{2}\rho^{\frac{1}{2}}\sin\theta)$$

with the Jacobian $J = \frac{1}{8R}$.

4 | THE FULLY DISCRETE PROBLEM

Let N_d be the dimension of $\mathcal{X}_h$ and we introduce a basis $\{\phi_i\}_{i=1}^{N_d}$ for the finite dimensional space $\mathcal{X}_h$. We write the trial functions $u_h \in \mathcal{X}_h$ as linear combination of basis functions with time-dependent coefficients as follows

$$u(\mathbf{x},t) \approx u_h(\mathbf{x},t) = \sum_{j=1}^{N_d} U_j(t)\,\phi_i(\mathbf{x}). \tag{9}$$

Replacing in (7) u_h by (9) and v_h by ϕ_j we obtain a linear first order equation that reads

$$M\,\dot{U}(t) + A\,U(t) = F(t), \quad \forall\, t \in [0,T], \qquad U(0) = U_0 \tag{10}$$

where M is the capacitance matrix, A is the conduction matrix, F is the source vector, $U(t)$ (resp., U_0) is the vector of dofs $U_j(t)$ (resp., $U_{0,j}$) for the temperature field at the time $t > 0$ (resp., $t = 0$) and the superposed dot indicates time differentiation. Let us subdivide the interval $[0,T]$ into M subintervals of amplitude $\delta t = T/M$ and define $t_m = m\Delta t$, for $m = 1, M$ with $t_0 = 0$. One problem with the numerical simulation is that the stability criterion is generally $\delta t \leq \delta t_{diff} = h^2/(2c_{\|})$. An explicit scheme has to verify this time step condition at any time, which is very restrictive, especially for the problem we are considering. Implicit numerical solvers are favoured in the present situation. We then use the second-order Gear (BDF2) scheme

$$(M + \frac{2}{3}\,\delta t\,A)\,U^{m+1} = \frac{4}{3}M\,U^m - \frac{1}{3}\,M\,U^{m-1} + \frac{1}{3}\,\delta t\,F^{m+1}, \quad m \geq 1, \tag{11}$$

with U^1 computed by solving $(M + \delta t\,A)\,U^1 = M\,U^0 + \delta t\,F^1$, resulting from an implicit Euler scheme (BDF1) applied to (10), and $U^0 = U_0$, by the initial condition.

5 | COMPUTATIONAL RESULTS AND DISCUSSION

We present results on the numerical diffusion of two C1 finite element discretizations of the weak problem associated with (1) for different values of ϵ and various meshes that are either aligned or not with $\mathbf{b}$.

5.1 | Testing numerical accuracy for the stationary problem

We start by checking, separately, the accuracy of the rHCT and HB FEs when adopted to approximate the solution of the stationary problem

$$\nabla \cdot (\mathbb{D} \nabla u) + f = 0 \qquad \forall \mathbf{x} \in \Omega = [0,1]^2, \tag{12}$$

with $c_\perp = 1$, $c_\parallel \in \{1, 10^4, 10^8\}$ and $\mathbb{D}$ involving $\mathbf{b} = (\frac{y}{R}, -\frac{x}{R})$, with $R^2 = x^2 + y^2$ (we set $\mathbf{b} = \mathbf{0}$ at $(0,0)^\top$). For a given solution u of problem (12), we can compute the Dirichlet boundary value u_∂ by considering the restriction $(u)_{|\partial\Omega_h}$ and the right-hand side f in Ω_h as follows. Being

$$\mathbb{D}\,\nabla u = (c_\parallel - c_\perp) \begin{pmatrix} b_1^2 & b_1\,b_2 \\ b_1\,b_2 & b_2^2 \end{pmatrix} \begin{pmatrix} \partial_x u \\ \partial_y u \end{pmatrix} + c_\perp \begin{pmatrix} \partial_x u \\ \partial_y u \end{pmatrix}$$

from $f = -\nabla \cdot (\mathbb{D} \nabla u)$ we get, respectively,

$$\begin{aligned} f \;=\; & -\left[(c_\parallel - c_\perp)\, b_1^2 + c_\perp\right] \partial_{xx} u - 2\,(c_\parallel - c_\perp)\, b_1\, b_2\, \partial_{xy} u - \left[(c_\parallel - c_\perp)\, b_2^2 + c_\perp\right] \partial_{yy} u \\ & -(c_\parallel - c_\perp)\left[\partial_x (b_1^2) + \partial_y (b_1\, b_2)\right] \partial_x u \;-\; (c_\parallel - c_\perp)\left[\partial_x (b_1\, b_2) + \partial_y (b_2^2)\right] \partial_y u. \end{aligned}$$

Now, we choose $u(x,y) = \sin(2\,\pi\,x)\,\sin(2\,\pi\,y)$ as solution of (12). We use different meshes τ_{h_i} whose elements T_k have size $h_i = 1/(nr)_i$, with nr_i equal to fixed values (see x-axis values in Figures 2, 3). For rHCT FEs, we use a uniform mesh of triangles T_k whereas for HB FEs the mesh elements T_k are squares with straight edges.

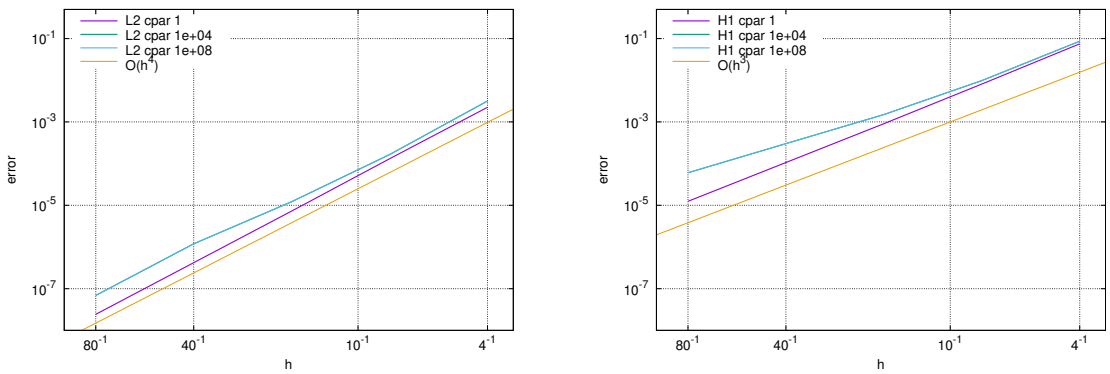

Figure 2 Logarithmic representation of the error in the L^2 norm (left) and H^1 seminorm (right), together with the asymptotic slope, for different values of the diffusion coefficient $c_\parallel$ (cpar in the legend) and the coefficient $c_\perp = 1$, with HB FEs.

The error with rHCT FEs in the $L^2(D)$ norm (resp., the $H^1(D)$ seminorm) behaves as $O(h^p)$, with $p = 3$ (resp., $p = 2$) with $h = \max_{T\in\tau} \mathrm{diam}\,(T)$, being τ the triangular mesh covering $\overline{\Omega}$. On the left (resp. right) side of Fig. 3, we report the errors computed in the same norms for P1 (resp., rHCT) FEs, and we see a difference of exactly one order in the drawn convergence rates. In both cases, computations are sensible to high values of $c_\parallel$. In the Figures, the lines for $c_\parallel = 1$ or $c_\parallel = 10^4$ are superposed. The theoretical error with HB FEs in the L^2 norm (resp., H^1 seminorm) behaves as $O(h^p)$, with $p = 4$ (resp., $p = 3$) with h the size of the mesh elements covering

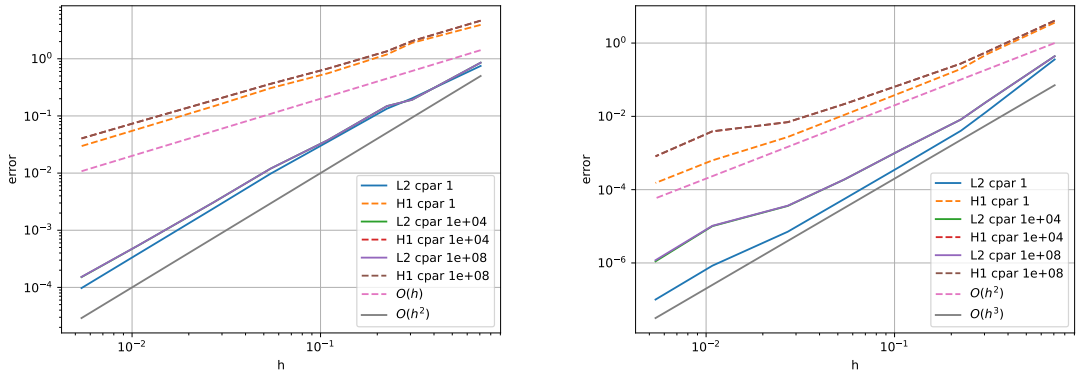

Figure 3 Logarithmic representation of the error in the L^2 norm (solid line) and H^1 seminorm (dashed), together with the asymptotic slope, for different values of the diffusion coefficient $c_\parallel$ (cpar in the legend) and the coefficient $c_\perp = 1$: P1 FEs (left) and rHCT FEs (right).

$\bar{\Omega}_h$. This is confirmed numerically in Fig. 2. Again, the results obtained for $c_\parallel = 10^8$ are not confused with those obtained for $c_\parallel = 1$ or $c_\parallel = 10^4$.

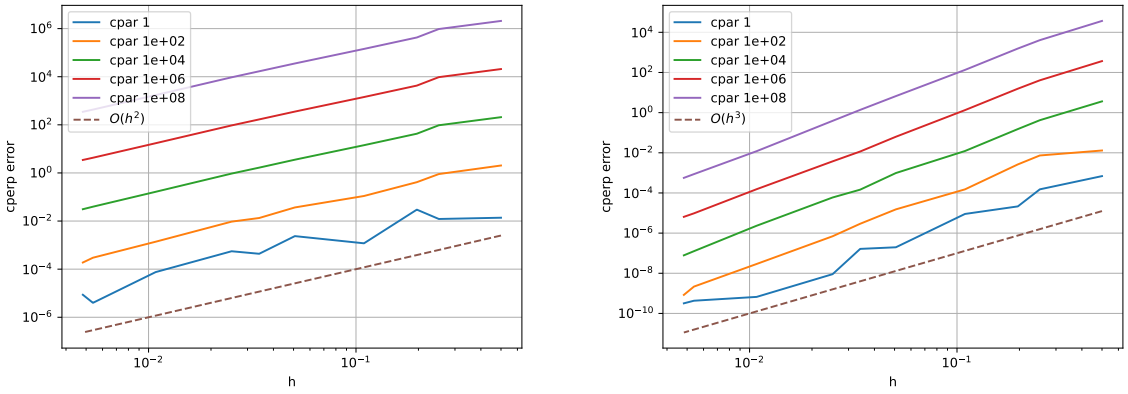

Figure 4 Logarithmic representation of the error $|\frac{1}{u(0,0)} - 1|$ with respect to h, for different values of $c_\parallel$ (cpar in the legend): P1 FEs (left) and rHCT FEs (right).

We complete the accuracy investigation by considering a rather classical benchmark suggested by Sovinec in 2001 to directly compare the numerically computed perpendicular diffusion to the exact perpendicular diffusion $c_\perp$ (see, e.g.,[30]). The stationary problem (12) in now set in $\Omega = [-0.5, 0.5]^2$. We choose the source term $f = 2\pi^2\,\psi$ with $\psi = \cos(\pi\,x)\,\cos(\pi\,y)$, and Dirichlet boundary conditions such that $u = \frac{1}{c_\perp}\psi$ is the solution. We impose a magnetic induction $\mathbf{b}$ tangent to ψ, namely $\mathbf{b} = (-\partial_y\psi, \partial_x\psi)/|\nabla\,\psi|$. When $c_\perp = 1$ and $c_\parallel \gg 1$, the inverse of the computed value $u(0,0)$ is a valid measure of the effective diffusion $c_\perp$. In Fig. 4 we present the results obtained

on a Cartesian grid with, for example, P1 and rHCT FEs, respectively. These results confirm the accuracy orders already obtained in the previous example and show a dependency of the error values on the anisotropy level.

5.2 | Testing numerical diffusion for the unstationary problem

In the square $\Omega_h = [-1,1]^2$, on a structured mesh of quadrangles and of triangles, we solve the unstationary problem with $f = 0$. The Dirichlet boundary value u_∂ is given by $(u_0)_{|\partial\Omega}$, the restriction of the initial solution u_0 at the boundary of Ω. We consider the step function u_0 that takes value 1 at points such that $|R - 0.6] \leq 0.1$ and 0 elsewhere in Ω_h. We set $c_\perp = 1$, $c_\parallel \in \{10^6, 10^8\}$ and $\mathbb{D}$ involving $\mathbf{b} = (\frac{y}{R}, -\frac{x}{R})$, with $R^2 = x^2 + y^2$ (as before, $\mathbf{b}(0,0) = \mathbf{0}$). Numerical diffusion yields smearings on the solution jumps and intensity overshoots (the function u_h reaches higher or lower values than the analytical ones), as schematized in Fig. 5 (left). This numerical error becomes important with the increase of $c_\parallel$, especially when the mesh is not aligned with the magnetic flow direction $\mathbf{b}$. This is visible in Fig. 6 (the rHCT FE solution is computed on a structured mesh of triangles) and in Fig. 7 (the HB FE solution is computed on a structured mesh of quadrangles). As soon as the mesh is aligned with the direction of the anisotropy, the numerical diffusion is highly reduced. In Fig. 8, rHCT FEs are applied in the domain $\Omega_h = C(\mathbf{0},1) \setminus C(\mathbf{0},0.01)$ on a mesh of triangles, built up layer by layer, in order to respect at maximum the anisotropy direction (see Fig. 5, left). Numerical diffusion has almost disappeared in Fig.9, since HB FEs are adopted in the domain $\Omega_h = C(\mathbf{0},1) \setminus C(\mathbf{0},0.01)$ on a mesh of curved quadrangles aligned with $\mathbf{b}$ (as shown in Fig. 5, right).

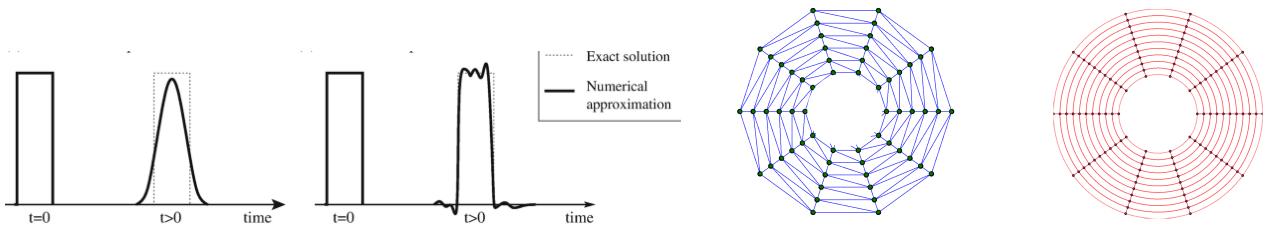

Figure 5 Left: Possible effects of numerical diffusion on a step function with time passing. Right: Simplified examples of meshes in the domain $\Omega_h = C(\mathbf{0},1) \setminus C(\mathbf{0},0.01)$. Straight triangles (blue) and curved quadrangles (red) are aligned with the field lines of $\mathbf{b} = (\frac{y}{R}, -\frac{x}{R})$.

In Fig. 10, we present the HB FE solution u_h of the unstationary problem computed in $\Omega_h = [-1,1]^2$ and in $\Omega_h = C(\mathbf{0},1) \setminus C(\mathbf{0},0.01)$, with homogeneous Dirichlet boundary conditions on $\partial\Omega_h$ and $f = 0$. The initial solution is again the step function. We make the assumption that $c_\perp = 0$, and we should obtain $u(\mathbf{x},t) = u_0(\mathbf{x})$ for all $t \in [0,T]$ and all $\mathbf{x} \in \bar{\Omega}_h$, by adapting the reasoning presented in Example 1. The fact of computing in an annulus is related to the impossibility of going up to the center of a disk with a mesh of curved quadrangular elements, aligned with $\mathbf{b} = (\frac{y}{R}, -\frac{x}{R})$. It can be seen that a mesh aligned with the circular anisotropy (bottom row) allows to keep $u_h \approx u$ whereas it is not the case on a Cartesian mesh (top row).

We test the numerical diffusion of the considered FE approximations in the case of a mesh associated with the Solov'ev equilibrium presented in Example 2. We thus compute in Ω_h defined by its frontier $\partial\Omega_h = \mathcal{C}(\mathbf{X}_0, r^0) \cup \{\mathbf{X} = (R_0\sqrt{R_c + 2a\cos\theta}\ ,\ aR_0\sin\theta)\ ,\ \theta \in [0, 2\pi]\}$

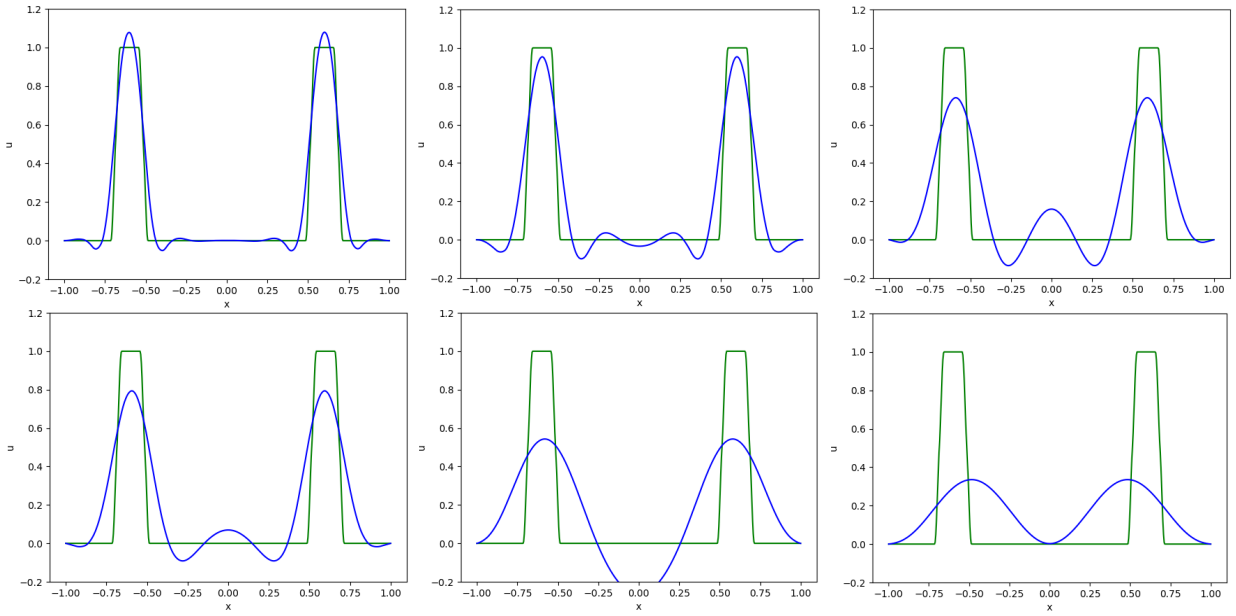

Figure 6 Case u_0 equal to the step function. Profile of the rHCT FE solution u for $c_{\parallel} = 10^6$ (top row) and $c_{\parallel} = 10^8$ (bottom row), $c_{\perp} = 1$, along the x-axis ($x = R$) inside $\Omega_h = [-1, 1]^2$ at $t = 10^{-6}$ s (left), at $t = 10^{-5}$ s (center), at $t = 10^{-4}$ s (right), on a structured mesh of $36 \times 36 \times 2$ triangles.

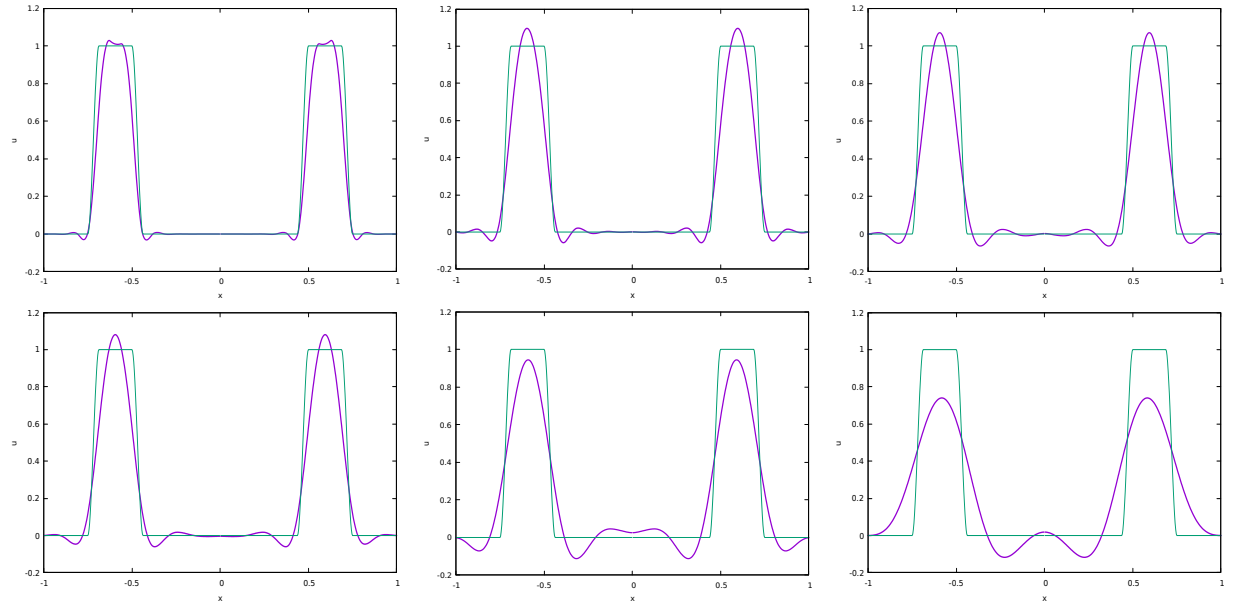

Figure 7 Case u_0 equal to the step function. Profile of the HB FE solution u for $c_{\parallel} = 10^6$ (top row) and $c_{\parallel} = 10^8$ (bottom row), $c_{\perp} = 1$, along the x-axis ($x = R$) inside $\Omega_h = [-1, 1]^2$ at $t = 10^{-6}$ s (left), at $t = 10^{-5}$ s (center), at $t = 10^{-4}$ s (right), on a structured mesh of 36×36 quadrangles.

where $\mathcal{C}(\mathbf{X}_0, r^0)$ is the circle of center $\mathbf{X}_0 = (R_c, 0)$, with $R_c = 1$ and radius $r^0 = 0.02$. Moreover, we set $a = 0.5$ and $R_0 = 1$ for which the domain is shown in Fig. 11.

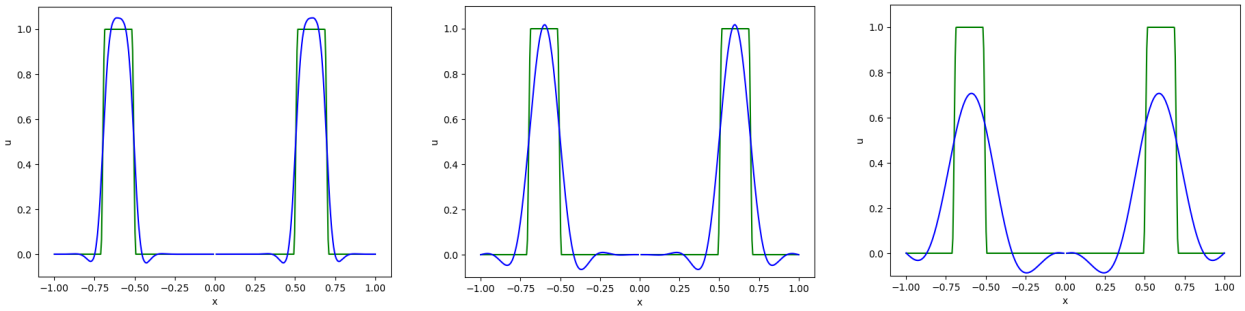

Figure 8 Case u_0 equal to the step function. Profile of the rHCT FE solution u for $c_{\parallel} = 10^8$, $c_{\perp} = 1$, along the x-axis ($x = R$) inside $\Omega_h = C(\mathbf{0}, 1) \setminus C(\mathbf{0}, 0.01)$ at $t = 10^{-6}$ s (left), at $t = 10^{-5}$ s (center), at $t = 10^{-4}$ s (right), on a structured mesh of $40 \times 50 \times 2$ triangles.

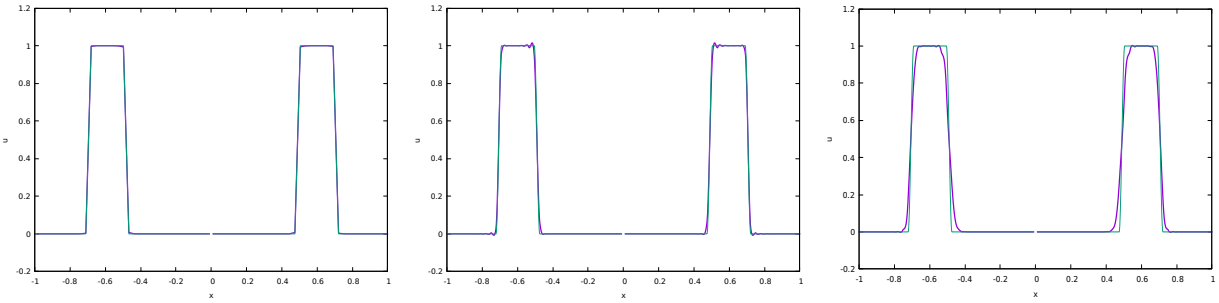

Figure 9 Case u_0 equal to the step function. Profile of the HB FE solution u_h for $c_{\parallel} = 10^8$, $c_{\perp} = 1$, along the r-axis inside $\Omega_h = C(\mathbf{0}, 1) \setminus C(\mathbf{0}, 0.01)$ at $t = 10^{-6}$ s (left), at $t = 10^{-5}$ s (center), at $t = 10^{-4}$ s (right), on a structured mesh of 36×36 curved quadrangles.

Problem (11) is solved with initial condition given by the pulse function $u_0 = 1 + e^{-\|\mathbf{x}-\mathbf{X}_0\|^2/\delta^2}$, centered in $\mathbf{X}_0 = (0.6, 0)$, with decay factor $\delta = 0.05$. The time step is $\delta t = 10^{-6}$ s, in order to visualise the phenomena occurring at the very first steps when $c_{\parallel} = 10^6$ and $c_{\perp} = 1$. The profile of $u_h(t, x, 0)$ for $x = r \in [0.02, 1.4]$ and $t = 0$ s (the initial condition), $t = 10^{-6}$ s (after one time step with the BDF1 scheme) and $t = 10^{-5}$ s (after ten time step with the BDF2 scheme), is considered. In Fig. 12 (left and center columns), the computed function u_h is obtained by using the rHCT FEs on the meshes of triangles shown in Fig. 11 (left and center, respectively), whereas, in Fig. 12, HB FEs are adopted on a mesh of curved quadrangles aligned with the surfaces of constant value for ψ, the Solov'ev equilibrium (see Fig. 11, right). For all the tests, the vector $\mathbf{b}$ is $\frac{1}{R}(-\partial_y\psi, \partial_x\psi)$, with R the distance from the tokamak axis (hence, $R = x$ here).

Numerical errors for the solution of problem (5) in the limit of large $c_{\parallel}/c_{\perp}$ have two effects: (1) the presence of unphysical temperature gradients along field lines, and (2) a finite heat flux perpendicular to field lines, proportional, at given temperature gradients, to $c_{\parallel}$. Both effects can be observed in Fig. 12. Effect (1) shows up as oscillations in the profile of $u_h(x, 0)$. Looking at the three results from left to right, we observe that these oscillations become less and less evident as soon as the mesh is more structured and aligned with $\mathbf{b}$. Effect (2) is visible, for example, in the quantity $\delta > 0$ such that $|x - 0.6| = \delta$ and $u_h(x, 0) = 1.02$. Indeed, we obtain, respectively, $\delta = 1$ on the unstructured mesh, 0.85 on the structured triangular mesh and 0.75 on the aligned quadrangular mesh. This means that u_h has diffused in the direction perpendicular to $\mathbf{b}$, and that the entity of this diffusion is more important when the unstructured mesh is considered.

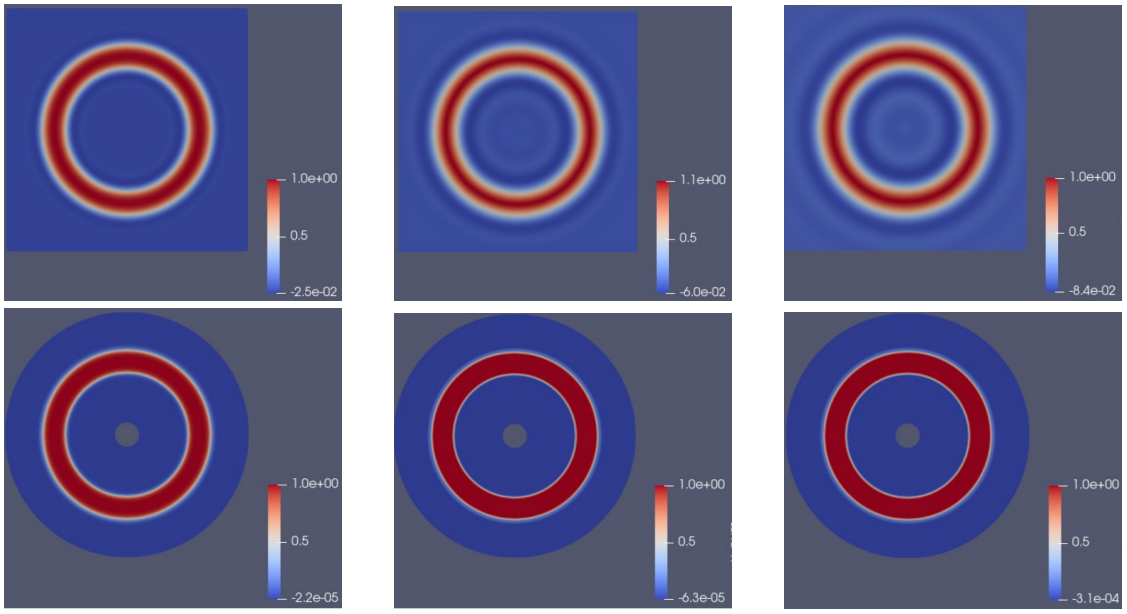

Figure 10 Case u_0 equal to the step function. Contours of the HB FE solution u_h for $c_{\|} = 10^4$, $c_{\perp} = 0$, inside $\Omega_h = [-1, 1]^2$ (top tow) and $\Omega_h = C(\mathbf{0}, 1) \setminus C(\mathbf{0}, 0.01)$ (bottom row) at $t = 10^{-6}$ s (left), at $t = 10^{-5}$ s (center), at $t = 10^{-4}$ s (right), on a structured mesh (top row) or on a curved one (bottom row) of quadrangles.

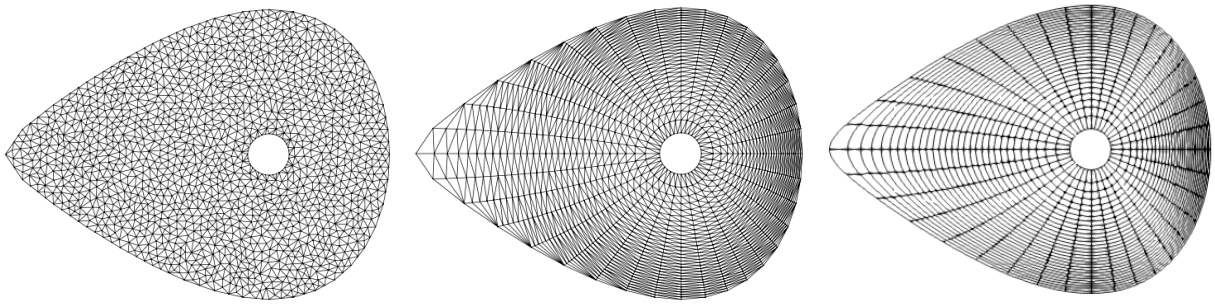

Figure 11 Examples of meshes in Ω_h: (left) unstructured non-aligned mesh of triangles, (center) structured mesh of triangles and (right) structured and aligned mesh of curved quadrangles. The Triangle software is run to create the mesh for rHCT FEs. For a HB FE mesh, coordinates and scales are built with the technique explained in [13].

6 | CONCLUSIONS

We have considered two FEs approaches, the rHCT and the HB ones, classically used in magneto-hydro-dynamic computations. Indeed, rHCT FEs are implemented in the `NICE` software[19] and HB FEs in the `JOREK` one[10,31], to obtain a $\mathcal{C}^1$ solution of the Grad-Shafranov equation in the plasma domain. Both codes are extensively used by the CEA in Cadarache to test different plasma discharge scenarii for the (under construction) tokamak ITER. We have coupled these two FE methods with a Gear finite difference scheme to solve a simplified but highly anisotropic temperature model equation. As soon as the mesh is adapted to the direction of the anisotropy, numerical diffusion is highly reduced. The two analysed FEs approaches thus remain excellent candidates for the numerical treatment of magnetically

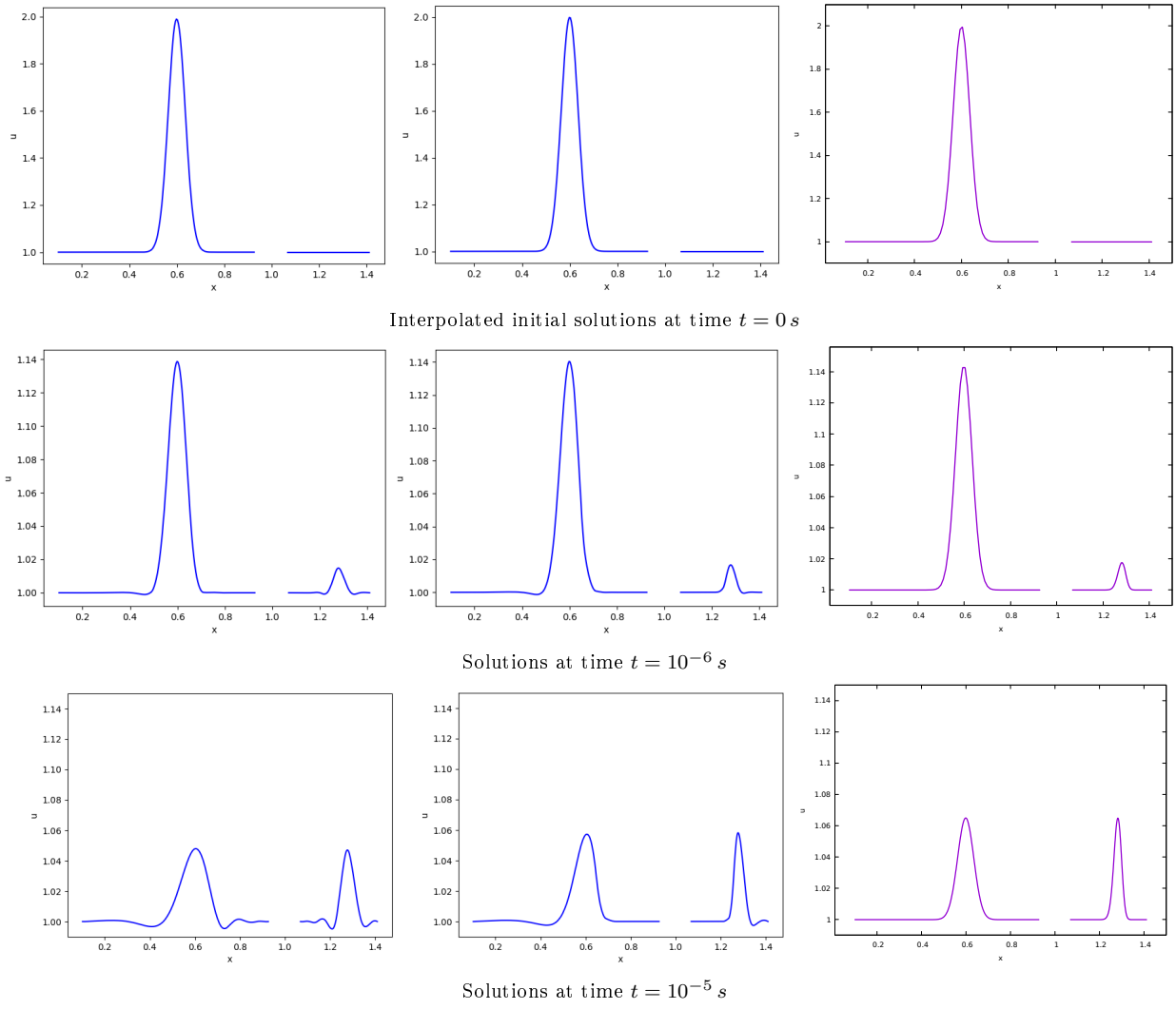

Figure 12 The pulse function along the r-axis inside Ω_h: rHCT on unstructured non-aligned straight triangles (left), rHCT on unstructured aligned straight triangles (center) and HB on aligned curved quadrangles (right).

confined plasma. However, specialized software rather solves reduced 1D models for those quantities (e.g., the temperature, the particle density) whose computation can be spoiled by numerical diffusion and reserve a 2D FE approach for the magnetic flux quantity. This work completes the ones described in [32,13] and future applications on reduced models are forthcoming.

ACKNOWLEDGMENTS

FR thanks INRIA for the delegation during which this work was accomplished. BF, HG and BN have worked within the framework of the EURO Fusion Consortium. The views and opinions expressed herein do not necessarily reflect those of the European Commission.

Financial disclosure

FR is supported by the French National Research Agency grant SISTEM (ANR-19-CE46-0005-03). BF, HG and BN have received funding from Euratom research and training programs 2014-2018, 2019-2020, 2021-2025 under the grant agreement N.633053.

Conflict of interest

The authors declare no potential conflict of interests.

Data availability statement

Data are available on request from the authors.

References

1. Blum J. Numerical Simulation and Optimal Control in Plasma Physics with Applications to Tokamaks. Series in Modern Applied MathematicsParis: Wiley Gauthier-Villars . 1989.

2. Francis Filbet CN, Yang C. Numerical study of a nonlinear heat equation for plasma physics. International Journal of Computer Mathematics 2012; 89(8): 1060–1082.

3. Isoardi L, Ciraolo G, Chiavassa G, et al. Modelling SOL flow pattern spreading in the edge plasma. Journal of Nuclear Materials 2009; 390-391: 388-391.

4. Pérez-Grande D, Gonzalez-Martinez O, Fajardo P, Ahedo E. Analysis of the Numerical Diffusion in Anisotropic Mediums: Benchmarks for Magnetic Field Aligned Meshes in Space Propulsion Simulations. Applied Sciences 2016; 6(11).

5. Braginskii S. Transport processes in a plasma. Review of Plasma Physics 1965; 1: 205-311.

6. Jardin S. Self-consistent solutions of the plasma transport equations in an axisymmetric toroidal system. Journal of Computational Physics 1981; 43(1): 31–60. doi: 10.1016/0021-9991(81)90110-8

7. Degond P, Deluzet F, Negulescu C. An Asymptotic Preserving Scheme for Strongly Anisotropic Elliptic Problems. Multiscale Modeling & Simulation 2010; 8(2): 645-666.

8. Degond P, Deluzet F, Lozinski A, Narski J, Negulescu C. Duality-based Asymptotic-Preserving method for highly anisotropic diffusion equations. Commun. Math. Sci. 2012; 10(1): 1-31.

9. Mentrelli A, Negulescu C. Asymptotic-Preserving scheme for highly anisotropic diffusion equations. J. Comput. Phys. 2012; 231(24): 8229-8245.

10. Czarny O, Huysmans G. Bézier surfaces and finite elements for MHD simulations. Journal of Computational Physics 2008; 227(16): 7423 - 7445. doi: http://dx.doi.org/10.1016/j.jcp.2008.04.001

11. Giorgiani G, Bufferand H, Ciraolo G, Serre E, Tamain P. A magnetic-field independent approach for strongly anisotropic equations arising plasma-edge transport simulations. Nuclear Materials and Energy 2019; 19: 340-345.

12. Heumann H, Rapetti F. A finite element method with overlapping meshes for free-boundary axisymmetric plasma equilibria in realistic geometries. Journal of Computational Physics 2017; 334: 522-540.

13. Bhole A, Nkonga B, Guillard H, Rapetti F. Coupling finite elements of class C1 on composite curved meshes for second order elliptic problems. Int. J. Numer. Meth. in Fluids 2023; 96(2): 209-230.

14. Krishnamurthy A, Gonzales M, Sturgeon G, Segars W, McCulloch A. Biomechanics simulations using cubic Hermite meshes with extraordinary nodes for isogeometric cardiac modeling. Computer Aided Geometric Design 2016; 43: 27–38.

15. Hou TY, Wu XH. A Multiscale Finite Element Method for Elliptic Problems in Composite Materials and Porous Media. Journal of Computational Physics 1997; 134(1): 169-189.

16. Vazquez JL. The Porous Medium Equation: Mathematical Theory. Oxford University Press . 2006.

17. Clough R, Tocher J. Finite element stiffness matrices for analysis of plates in bending. In: ; 1965; Air Force Inst of Tech., Wright Patterson A.F Base, Ohio.

18. Freidberg JP. Plasma Physics and Fusion Energy. Cambridge . 2007.

19. Faugeras B. An overview of the numerical methods for tokamak plasma equilibrium computation implemented in the NICE code. Fusion Engineering and Design 2020; 160: 112020.

20. Artaud J, Basiuk V, Imbeaux F, et al. The CRONOS suite of codes for integrated tokamak modelling. Nuclear Fusion 2010; 50(4): 043001.

21. Jardin S. Computational methods in plasma physics. Boca Raton, FL : CRC Press/Taylor & Francis . 2010.

22. Gros G, Faugeras B, Boulbe C, Artaud JF, Nouailletas R, Rapetti F. Numerical simulation of tokamak plasma equilibrium evolution. Research Report RR-9548, INRIA; 2024. https://hal.science/hal-04589897.

23. Baschetti S, Bufferand H, Ciraolo G, et al. A k-ϵ model for plasma anomalous transport in tokamaks: closure via the scaling of the global confinement. Nuclear Materials and Energy 2019; 19: 200–204.

24. Drescher L, Heumann H, Schmidt K. A High Order Method for the Approximation of Integrals Over Implicitly Defined Hypersurfaces. SIAM Journal on Numerical Analysis 2017; 55(6): 2592-2615. doi: 10.1137/16M1102227

25. Federer H. Geometric Measure Theory. Springer-Verlag . 1969.

26. Blum J, Le Foll J. Plasma equilibrium evolution at the resistive diffusion timescale. Computer Physics Reports 1984; 1(7-8): 465–494. doi: 10.1016/0167-7977(84)90013-3

27. Quarteroni A, Valli A. Numerical approximation of partial differential equations. 23 of Springer Series in Computational Mathematics. Berlin: Springer-Verlag . 1994.

28. Ciarlet PG. The Finite Element Method for Elliptic Problems. Amsterdam: North-Holland Publishing Co. . 1978. Studies in Mathematics and its Applications, Vol. 4.

29. Bernardou M, Hassan K. Basis functions for general Hsieh-Clough-Tocher triangles, complete or reduced. Research Report RR-0005, INRIA; 1980.

30. Günter S, Yu Q, Krüger J, Lackner K. Modelling of heat transport in magnetised plasmas using non-aligned coordinates. Journal of Computational Physics 2005; 209(1): 354-370. doi: https://doi.org/10.1016/j.jcp.2005.03.021

31. Bhole A, Nkonga B, Pamela S, Huijsmans G, Hoelzl M. Treatment of polar grid singularities in the bi-cubic Hermite-Bézier approximations: Isoparametric finite element framework. Journal of Computational Physics 2022; 471: 111611.

32. Boulbe C, Faugeras B, Gros G, Rapetti F. Tokamak Free-Boundary Plasma Equilibrium Computations in Presence of Non-Linear Materials. J. Sci. Comput. 2023; 96(2).

How to cite this article: F. Faugeras, H. Guillard, B. Nkonga, and F. Rapetti (2024), On the behavior of two C1 finite elements versus anisotropic diffusion